New Journal of Physics
The open-access journal for physics

Confinement and propagation characteristics of subwavelength plasmonic modes

R F Oulton[1], G Bartal[1], D F P Pile[2] and X Zhang[1,3,4]

[1] NSF Nano-scale Science and Engineering Center, 3112 Etcheverry Hall, University of California, Berkeley, CA 94720, USA

[2] Applied Optics Program, School of Physical and Chemical Sciences, Queensland University of Technology, GPO Box 2434, Brisbane, QLD 4001, Australia

[3] Materials Sciences Division, Lawrence Berkeley National Laboratory, 1 Cyclotron Road, Berkeley, CA 94720, USA

E-mail: xiang@berkeley.edu

New Journal of Physics **10** (2008) 105018 (14pp)
Received 22 June 2008
Published 28 October 2008
Online at http://www.njp.org/
doi:10.1088/1367-2630/10/10/105018

Abstract. We have studied subwavelength confinement of the surface plasmon polariton modes of various plasmonic waveguides and examined their relative merits using a graphical parametric representation of their confinement and propagation characteristics. While the same plasmonic phenomenon governs mode confinement in all these waveguides, the various architectures can exhibit distinctive behavior in terms of effective mode area and propagation distance. We found that the waveguides based on metal and one dielectric material show a similar trade-off between energy confinement and propagation distance. However, a hybrid plasmon waveguide, incorporating metal, low index and high index dielectric materials, exhibits longer propagation distances for the same degree of confinement. We also point out that plasmonic waveguides with sharp features can provide an extremely strong local field enhancement, which is not necessarily accompanied by strong confinement of the total electromagnetic energy. In these waveguides, a mode may couple strongly to nearby atoms, but suffer relatively low propagation losses due to weak confinement.

[4] Author to whom any correspondence should be addressed.

Contents

1. Introduction

Nano photonics research has seen a surge in sub-micron scale components capable of transporting and manipulating light. While many of these components are physically smaller than the wavelength of light in vacuum, their electromagnetic field confinement is typically limited by diffraction. Squeezing light into regions of space much smaller than the diffraction limit is possible by using a number of waveguide architectures that store part of the light's energy as plasma oscillations at the interfaces of metal and dielectric materials [1]. These so-called surface plasmon polariton (SPP) modes are capable of confining light to sizes that are much smaller than the diffraction limit, and despite intrinsic losses, may transmit light for up to 100 wavelengths at telecommunications frequencies.

Candidates for strong sub-wavelength light transport include SPPs of metal cylinders of circular (cylinder plasmon polaritons (CyPP)) [2, 3] or square cross-section [4], coupled metal nano-particles [5], metal wedges (wedge plasmon polaritons (WPPs)) [6]–[8], channels in metal surfaces (channel plasmon polaritons (CPPs)) [9]–[11] and hybrids of conventional dielectric waveguides (hybrid plasmon polaritons (HPP)) [12]. While these plasmonic waveguides operate on the same plasmonic phenomenon, the various architectures apparently exhibit different behavior in terms of confinement, propagation distance and the trade-off between the two. Understanding these differences is naturally relevant to their future application as visible nano-scale light sources [13, 14] as well as optical interconnects [15].

In this work, we have compared the confinement and propagation characteristics of WPP, CPP, CyPP and HPP waveguides, shown schematically in figure 1, using a graphical parametric representation. This is essentially a graphical figure of merit that allows us to identify the favorable plasmonic architectures without obscuring the absolute values of confinement and propagation distance. Such a representation is important as these waveguide plasmonic characteristics may vary by orders of magnitude for the range of possible structural parameters.

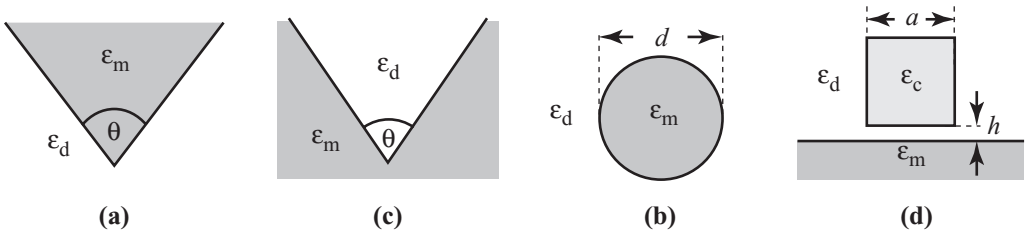

Figure 1. Schematics of plasmon supporting waveguides under investigation: (a) metal wedge [6, 7]; (b) groove in metal plane [9, 10]; (c) metal cylinder [3]; and (d) hybrid of dielectric and plasmon waveguides [12].

While the propagation distance of a mode is well defined, the available measures of mode area, inherited from conventional waveguide theory, are somewhat inconsistent when applied to plasmonic modes. This is because plasmonic waveguides can have sharp features that lead to rapid or discontinuous sub-wavelength variations in the shape of a mode, which is atypical in conventional diffraction limited waveguides. So for example, the notion of full width at half maximum as a measure of mode size is most relevant to Lorentzian lineshapes; but using it to measure the size of a plasmonic mode, whose field intensity may vary by many orders of magnitude within a small distance, can lead to uncertainty about the true extent of the field distribution.

In order to consistently quantify the mode confinement, we have used four measures of effective mode area. We have shown that each measure can lead to a different conclusion about the absolute and relative confinement strengths. Consequently, we emphasize the underlying relevance of each measure in gauging a particular physical effect. Two measures that are frequently used in the literature relate to the spontaneous emission enhancement of nearby atoms and the statistical measure of the overall localization of the electromagnetic field. The third measure, the area in which exactly half of a mode's energy resides, allows us to consistently compare the degree of overall energy confinement regardless of the shape of the mode. Finally, the fourth is the commonly used e^{-1} field criterion to gauge the extent of the mode distribution.

2. Plasmonic waveguides

We begin by briefly outlining the physical principles of WPP, CPP, CyPP and HPP waveguides.

WPPs [6]–[8] and CPPs [9]–[11] are the eigenmodes of metal wedges and grooves, respectively. The electromagnetic fields of these modes are maximal near the tips of the respective structures, as shown in the energy density maps in figures 2(a) and (b). These strongly localized plasmonic modes arise from the increased interaction strength of the surface plasma oscillations on the adjacent sidewalls and the specific geometry near the tip, which results in an effective graded index confinement. CPPs arise from strong sidewall interaction across an air gap leading to confinement within the groove that spreads out from the tip (figure 2(b)). Likewise, WPPs arise from the weaker coupling of surface plasma oscillations across the metal wedge. Since coupling of the electric charges is strongest near the narrowest region of the gap (for CPPs) and film (for WPPs), the tip's geometry strongly influences the properties of the mode; for example, sharp tip radii, ρ, and small sidewall angles, θ, lead to strong local

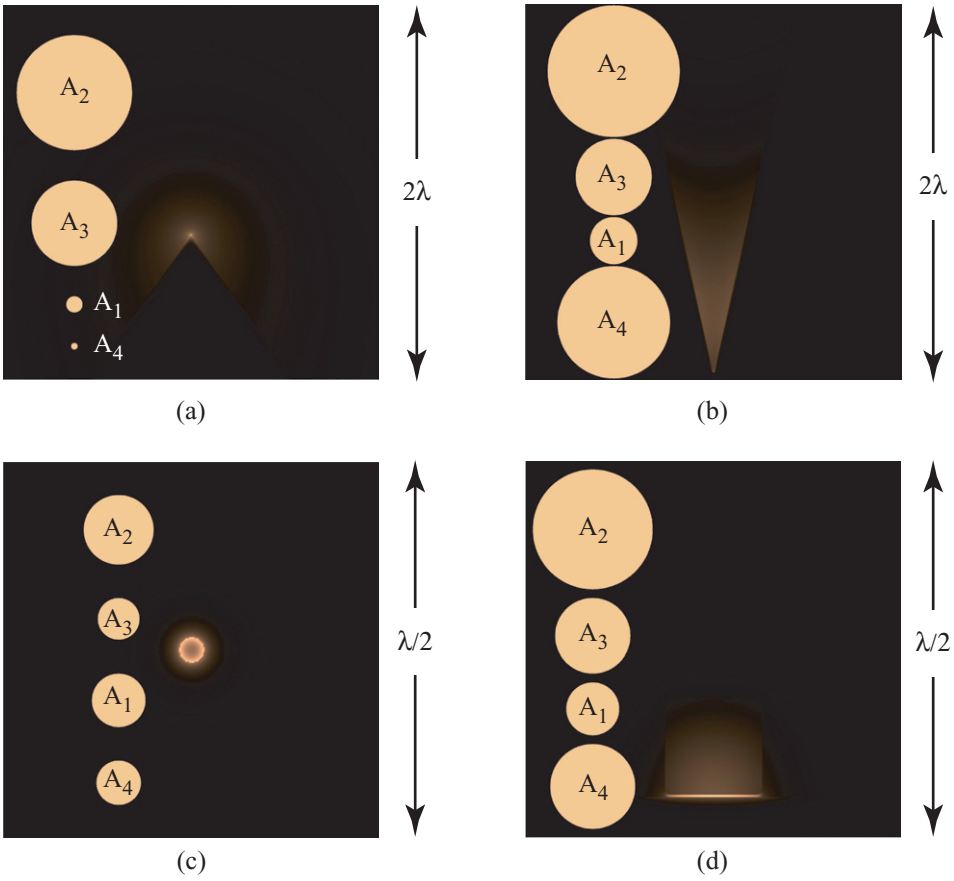

Figure 2. Distributions of (a) $\sqrt{W(\mathbf{r})}$ of WPP mode for $\theta = 70^\circ$ and $\rho_{\text{tip}} = 5\,\text{nm}$ [8]; (b) $W(\mathbf{r})$ of CPP modes for $\theta = 25^\circ$ and $\rho_{\text{tip}} = 5\,\text{nm}$; (c) $W(\mathbf{r})$ of CyPP modes for $d = 50\,\text{nm}$; and (d) $W(\mathbf{r})$ of HPP mode for $a = 200\,\text{nm}$ and $h = 5\,\text{nm}$. The disci within each panel show the effective size of the mode using the four measures, A_1, A_2, A_3 and A_4. Note that the plot regions of (a) and (b) are $4\times$ larger than (c) and (d) and so the disci within these panels must be scaled accordingly. In each plot, $\lambda = 1550\,\text{nm}$ is the vacuum wavelength. The scale of each plot is displayed in units of the vacuum wavelength, $\lambda = 1550\,\text{nm}$.

enhancement of the field at the tip. On the other hand, blunt tips and large sidewall angles cause a loss of confinement and mode cut-off.

CyPPs are the modes of isolated metal cylinders embedded in dielectric media. These modes were highlighted early on as possessing strong sub-wavelength characteristics [2, 3]. More recently, experimental demonstrations have shown that these characteristics are indeed observable through the spontaneous emission of quantum dots near metal nanowires [16, 17]. Here, the confinement arises from the capacitive coupling of surface plasma oscillations across the metallic cylinder core leading to energy density distributions as shown in figure 2(c). The confinement is controlled by the cylinder diameter, d.

Finally, the hybrid waveguide [12] is a composite of a rectangular high contrast dielectric waveguide and a plasmon supporting metal–dielectric interface separated by a thin dielectric gap. The coupling between the plasmonic and waveguide modes allows confinement within

the gap, shown in figure 2(d). This type of structure has potentially favorable confinement and propagation characteristics due to the involvement of the low loss dielectric waveguide. We evaluate this assertion in more detail in this paper. We control the confinement of this structure using the dielectric waveguide side length, a, and the thickness, h, of the dielectric gap region. Optimal confinement occurs for $a \simeq 200\,\text{nm}$ [12] and for small h. For large h, the metal plane and dielectric waveguide decouple leaving an essentially lossless dielectric waveguide. Here, we only consider the variation with respect to h and use $a = 200\,\text{nm}$ throughout.

The physical principles governing the operation of WPP, CPP, CyPP and HPP waveguides are well established. Therefore, we refer the reader to the excellent articles cited for more detailed discussions [2]–[12].

In order to ensure a fair comparison of these waveguides, identical metal and dielectric parameters are used for the telecommunications wavelength of $\lambda = 1550\,\text{nm}$. Here, the permittivity of silver is $\varepsilon_\text{m} = -129 + 3.3\text{i}$ [18], the permittivity of the host dielectric is $\varepsilon_\text{d} = 2.25$ (e.g. SiO_2) and the permittivity of the high dielectric waveguide in the HPP case is $\varepsilon_\text{c} = 12.25$ (e.g. silicon). In this study, all waveguides were analyzed numerically using finite element software[5] except the metal cylinder, which was treated analytically [19].

3. Measures of confinement and propagation

Plasmonic waveguides provide a route to generating extremely localized electromagnetic fields; however, the metal constituents impose an intrinsic cost on the distance these fields can travel. While the propagation has a straightforward definition, we have already discussed in the introduction the potential difficulties in defining a practical measure of the confinement. In this section, we provide definitions for the propagation distance and mode area, and in the following section, we examine their trade-off.

The field distributions of the plasmonic modes of the various waveguide structures maintain their shape in the plane, while propagating harmonically in the $\hat{z}$-direction so that all field components vary as $\exp(\text{i}\beta z - \text{i}\omega t)$. The propagation constant, β, is a complex number that describes both a mode's effective wavelength and attenuation as it propagates. The propagation distance, Λ, is defined as the distance a mode travels before decaying to e^{-1} of its original power,

$$\Lambda = \frac{1}{2\text{Im}\{\beta\}}. \tag{1}$$

There are a number of ways to gauge a mode's confinement by calculating the effective area of its distribution. For example, one could devise a *statistical measure* requiring integration of a property of the electromagnetic field (e.g. the energy density) over the cross section of the waveguide. However, when the confinement affects an actual physical process (e.g. the Purcell effect [20, 21]), a *phenomenological measure* would be more desirable. Moreover, statistical measures are sensitive to distribution, potentially leading to inconsistent results for different mode distributions. We therefore use a third and quite distinct measure that is based on a common feature of all waveguide modes: it is simply the area in which exactly half of a mode's energy resides. We have also examined the commonly used method of evaluating the mode area

[5] We used the finite element software FEMLab 3.4 by Comsol. The eigenmode solver was used with scattering boundary conditions. Convergence tests were performed to ensure that the numerical boundaries do not interfere with the mode solutions.

based on the region in which the mode energy drops to e^{-2} of its peak value. In the following section, we compare these measures of mode confinement for each waveguide, and show that they can lead to very different values for the effective mode area.

The first effective mode area, A_1, is the ratio of a mode's total energy density per unit length and its peak energy density,

$$A_1 = \frac{1}{\mathrm{Max}\{W(\mathbf{r})\}} \int_{A_\infty} W(\mathbf{r})\, \mathrm{d}A, \tag{2}$$

where $W(\mathbf{r})$ is the energy density,

$$W(\mathbf{r}) = \frac{1}{2}\mathrm{Re}\left\{\frac{\mathrm{d}[\omega\varepsilon(\mathbf{r})]}{\mathrm{d}\omega}\right\}|\mathbf{E}(\mathbf{r})|^2 + \frac{1}{2}\mu_0|\mathbf{H}(\mathbf{r})|^2. \tag{3}$$

$|E(\mathbf{r})|^2$ and $|H(\mathbf{r})|^2$ are the electric and magnetic fields, $\varepsilon(\mathbf{r})$ is the electric permittivity, and μ_0 is the vacuum magnetic permeability. Interestingly, A_1 is in fact inversely proportional to the spontaneous emission rate enhancement, or the Purcell factor, F_p, of an atom placed at the mode's peak energy density (see appendix). For this reason, it is a widely used measure of mode area in the literature [12, 14, 21].

$$F_\mathrm{p} \sim \frac{1}{2\pi}\frac{A_0}{A_1}, \tag{4}$$

where $A_0 = (\lambda/2)^2$ is the diffraction limited area of vacuum.

The second measure, A_2, is a statistical measure,

$$A_2(F(\mathbf{r})) = \frac{\left[\int_{A_\infty} F(\mathbf{r})\, \mathrm{d}A\right]^2}{\int_{A_\infty} F(\mathbf{r})^2\, \mathrm{d}A}, \tag{5}$$

where $F(\mathbf{r})$ is a property of the mode's electromagnetic field. Here, we use the total energy density, $F(\mathbf{r}) = W(\mathbf{r})$, to evaluate A_2 instead of the more commonly used electric field intensity, $|E(\mathbf{r})|^2$. The use of energy density in the formula provides an indication of the complete electromagnetic size of the mode and allows us to compare this measure with the others that we are investigating. While this measure has seen limited use for plasmonics waveguides [15], it has a firm foundation in optical fiber theory [22].

Both A_1 and A_2 are appealing as they are easily evaluated from arbitrary field distributions. However, care must be taken when using them to compare plasmonic waveguides: A_1 depends on the peak energy density, so its value may not reflect the true extent of a mode's field distribution, where rapid field variations over small distances occur. Such variations are common in plasmonic components, especially at the sharp tips of WPP and CPP waveguides. While A_1 can be useful to quantify local field enhancement (e.g. the Purcell effect), A_2 should be a better measure of the true spatial extent of a mode. In the case of Gaussian beams it provides a measure of the area, πr_0^2, where the Beam radius r_0 is half the standard deviation, however, it is unclear how a plasmonic mode's energy density distribution would affect the result.

The aim of defining the third effective mode area, A_3, is to consistently gauge confinement for arbitrary field distributions. This is possible provided the definition is based on a common feature of all distributions. We propose to evaluate the minimum area in which a set proportion, η, of a mode's energy resides. Since the measure does not depend on the peak value of the field, it should be less sensitive to rapid field variations than A_1. Furthermore, since η is generic to any field distribution, A_3 should also be a geometry-independent measure of confinement. As there

is no explicit formula for this calculation, it requires us to solve the following minimization problem,

$$A_3 = \min_{f(\mathbf{r})} \int_{A_\infty} f(\mathbf{r})\, \mathrm{d}A,$$
$$\text{s.t.} \int_{A_\infty} [f(\mathbf{r}) - \eta]\, W(\mathbf{r})\, \mathrm{d}A = 0, \tag{6}$$

where $f(\mathbf{r})$ is some unknown shape function that encompasses a fraction η of the mode's energy density and $\eta = 0.5$ in the current study. Solving for $f(\mathbf{r})$ in an arbitrary plasmonic geometry would be an unnecessarily complicated task, so we have devised a straightforward approximation, which we anticipate will work for most modal field distributions. Here, we assume that the optimum $f(\mathbf{r})$ is a step function bounded by a constant energy density contour, W_0, of the mode. To find A_3, we iteratively solve the minimization problem of equation (6) using,

$$f(\mathbf{r}) = 0, \quad \text{if } W(\mathbf{r}) < W_0,$$
$$f(\mathbf{r}) = 1, \quad \text{if } W(\mathbf{r}) \geqslant W_0, \tag{7}$$

where W_0 corresponds to the contour containing η of the mode's energy. A_3, follows from integration over the shape function, $f(\mathbf{r})$ in equation (6). We can also use equations (6) and (7) to evaluate the fourth and final definition of mode area, A_4. By choosing, $W_0 = \gamma \max\{W(\mathbf{r})\}$, we can compute the area corresponding to when the peak energy density decays by a factor γ. This measure is widely used in the literature although the choice of γ is not so consistent, with values such as e^{-2} [3, 4, 23], $1/10$ [7, 8] or $1/2$ [10]. In this paper, we consider $\gamma = e^{-2}$. Despite its widespread use, we will show that A_4 is just as inconsistent as A_1 and can lead to significant underestimation of the true energy confinement of a plasmonic mode.

Figure 2 presents the energy density distributions of the fundamental modes of the plasmonic structures under investigation. Alongside, we illustrate the strength of confinement according to the four aforementioned measures, A_1, A_2, A_3 and A_4, where the radius of each discus, r_i, is chosen such that $A_i = \pi r_i^2$. Interestingly, not only are there stark differences between each measure of a field distribution, but the choice of measure also determines which waveguide has the strongest confinement. For example, the result of A_1 and A_4 for WPPs and CPPs differ dramatically; while A_2 and A_3 are much closer in value. In fact, according to A_1 and A_4, WPPs have the stronger confinement, whereas according to A_3, it is the CPPs that prove favorable. The same story is seen when comparing HPPs and CyPPs; A_1 indicates that HPPs and CyPPs have similar confinement, but A_3 shows that it is much stronger for CyPPs. Furthermore, the differences between the field distributions and their associated effective mode areas are quite striking. In particular, WPPs are far more spread out than their field distribution suggests, even though we have plotted $\sqrt{W(\mathbf{r})}$ in figure 2(a).

We have compared the various measures of mode confinement more thoroughly in appendix B, to which we refer the reader for a more detailed appraisal. Here, we merely summarize the capabilities of A_1, A_2 and A_4 for measuring confinement. The result of A_1 is typically the smallest since rapid field variations in small distances can give the impression that a mode's field is tightly confined, while most of the energy resides in a larger region of space; for example, the WPP distribution in figure 2 (a). We also show in appendix B that the tip radius of the wedge and groove structures predominantly affects the value of A_1, but not A_2 or A_3. Consequently, *the Purcell effect is not necessarily dependent on total mode localization, but on*

the local field enhancement. Measure A_2 displays the largest effective area for all the waveguides studied in this paper as it consistently represents more than 50% of a mode's energy. (See figure B.1, appendix B.) In this case, the A_2 measure is good for gauging the energy confinement; however, A_2 does not consistently represent the same amount of energy for all waveguides. A_4 appears to be the most inconsistent of all the measures of mode area and as a statistical measure, A_2, is more appealing due to a greater level of consistency. For WPPs, A_4 is susceptible to the rapid variation of the energy density within small distances and so underestimates the energy confinement, whereas for CPPs, it almost leads to an overestimate. Since A_4 is so inconsistent, we do not consider it further in this study. By definition, A_3 is the most reliable indicator of the relative energy confinement of different waveguides.

4. Parametric analysis of plasmonic waveguides

To understand the merits of the various plasmonic waveguide structures, it is necessary to have a direct method for comparing their confinement and propagation characteristics. Berini and co-workers define three dimensionless benefit-to-cost ratios as figures of merit [23]. One of these considers the square root of the confinement area as the benefit with the cost being the propagation loss. Here, we do not explicitly define a figure of merit, but rather choose to display the confinement area and propagation distance in a parametric plot. This graphical figure of merit allows direct comparison of any waveguide geometry, while maintaining a reference to the absolute values of confinement and propagation distance. Each plasmonic waveguide is represented by a trajectory along which a single geometrical property is varied, for example, the sidewall angle, θ, or the tip radius, ρ, for WPPs and CPPs; the diameter of the metal cylinder, d, for CyPPs; and the low index region's gap width, h, for HPPs. These parametric plots allow us to identify favorable plasmonic architecture without obscuring the absolute values of confinement and propagation distance.

4.1. The trade-off between confinement and propagation distance

Figure 3 shows parametric plots of normalized propagation distance, Λ/λ, versus normalized effective modes area, A_i/A_0, where $A_0 = (\lambda/2)^2$ is the diffraction limited area of vacuum.

Figure 3(a) depicts the A_1 measure, with the WPP, HPP and CyPP waveguides all having similar capabilities in terms of the overall confinement strength. Since A_1 indicates the strength of the Purcell effect (see appendix A), these modes can potentially couple strongly to atoms placed near the peak of their electric field. It is notable, however, that WPPs have a longer propagation distance for the same degree of confinement, making them all the more appealing for this purpose.

So why do WPPs have such favorable characteristics? This is because the propagation distance is determined by the total energy localization and not by the local field enhancement. While the metal tip induces a strong enhancement of the local field, most of the mode's energy resides in the lossless surrounding dielectric; hence its propagation loss is relatively small. We can clearly see this when using the measure A_3 (as shown in figure 3(b)), which shows that WPPs, CPPs and CyPPs, in fact, have similar total energy confinement versus propagation characteristics.

The trajectories of WPPs, CPPs and CyPPs in figure 3(b) suggest that the geometry of a plasmonic waveguide does not drastically affect the trade-off between confinement and

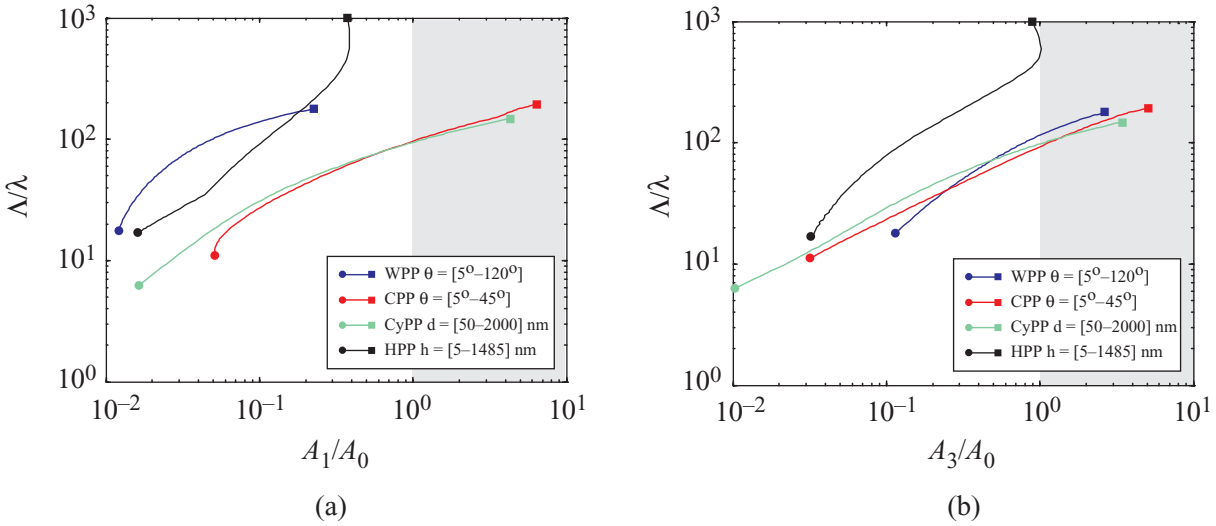

Figure 3. Parametric plots of normalized propagation distance $\Lambda\lambda$ and normalized effective mode area: (a) A_1/A_0 and (b) A_3/A_0. A similar trend results when considering the A_2 measure of mode area; however, A_2 does not represent the same proportion of mode energy for WPPs when compared with the other waveguides (for a comparison of A_2 and A_3, please see appendix B.)

propagation loss. Consequently, the hybrid plasmon waveguide is remarkable since it follows a completely different trajectory showing improved characteristics. The question of whether pure plasmonic geometries follow similar trade-offs between confinement and loss for the full range of design parameters remains an open one; however, it is clear that hybrid plasmonic waveguides offer improvements. These improvements become even more pronounced when the other geometries have semiconductor-based host materials [12]. While, high index dielectrics, such as semiconductors, introduce significant losses to pure plasmonic waveguides, these materials are intrinsic to the confinement mechanism in the hybrid geometry.

4.2. Nano-scale focusing capabilities

Recently, it was shown that energy can be efficiently concentrated into CyPPs [24, 25] and WPPs [7] by slowly varying the confinement parameter, d and θ, respectively, along the propagation direction. Figure 3(b) illustrates how this nano-scale focusing is possible: the range in confinement strength indicates how much of an increase in local energy density we can expect from the focusing; and the range in propagation distance shows how slowly a waveguide parameter can be varied to ensure the efficient transfer of energy to the nanoscale.

CyPPs, which were in fact the first geometry proposed for nanoscale focusing [24, 25], offer the strongest overall energy confinement of all the structures that we have considered. A particular strength of CyPPs is their broad range of mode areas, which spans almost three orders of magnitude, effectively linking conventional optical length scales with the nanoscale. CPPs are also interesting in this respect as they can span almost the same range in effective mode area. WPPs and HPPs provide just over one order of magnitude variation in effective mode area. In the case of WPPs this limits the effectiveness of the focusing. On the other hand, this capability

in HPPs provides an intriguing approach for linking conventional waveguide technology with subwavelength fields.

5. Summary

We have examined the confinement and propagation characteristics of four plasmonic waveguide geometries at the telecommunications wavelength, $\lambda = 1550$ nm. These plasmonic modes have quite distinct field distributions, which has made it very difficult to consistently gauge their confinement strength. We examined four approaches for calculating the effective mode area, i.e. a measure of confinement strength. However, none of these measures consistently concurred on either the absolute or relative confinement strengths of all the waveguide modes studied. It was therefore necessary to interpret each measure independently and emphasize its underlying relevance to a particular physical effect. A_1, which relates to the Purcell effect, depends heavily on the maximum local field enhancement and, as such can underestimate the extent of a mode's overall field distribution. A_2 is a decent statistical measure of the total energy confinement, but only A_3, by definition, is consistent in gauging the energy confinement of all the waveguides. The commonly used approach of evaluating the area, A_4, of the region in which the peak mode energy falls by e^{-2} was also found to be inconsistent.

To facilitate a detailed comparison of the various architectures, we have used a graphical approach to represent the confinement and propagation distance over a range of waveguide parameterizations. We summarize our main conclusions below.

5.1. WPPs

Wedge plasmons are the most irregular of the plasmonic waveguides investigated here as their properties are strongly dependent on the tip geometry. Fabrication challenges are potentially limiting for this geometry as the strongest confinement is reliant upon sharp tips and very acute wedge angles. Recent experiments at infrared wavelengths [8] have examined wedges with sidewall angle of 70° and tip radii approaching 25 nm, which yield impractical field confinement. Despite their unique field distribution, which leads to effective mode areas that are quite distinct from the other plasmonic modes studied, WPPs still follow a general trend of confinement versus propagation distance exhibited by all the conventional plasmonic waveguides studied. WPPs are potentially attractive for the enhancement of the atomic emission process near their tips. They can couple strongly to atoms due to very strong local field enhancements and may propagate long distances because their overall energy confinement is relatively weak.

5.2. CPPs

Channel plasmons are also quite strongly dependent on the radius of curvature of the tip and the steepness of the sidewalls (i.e. angle, θ). As in the case of WPPs, fabrication of the necessary sharp tip radii for strong confinement and steep sidewalls is impractical with current fabrication technology. To date, channel plasmons have only been observed for relatively weak confinement [10, 11] in the regime close to cut-off. Nevertheless, the results have been quite impressive with demonstration of plasmonic interferometers and ring resonators with nearly diffraction limited modes [11].

5.3. CyPPs

Despite the simplicity of the cylinder geometry, CyPPs perform extremely well in theory with respect to both spontaneous emission enhancement and overall energy confinement. In particular, the broad range of confinement strengths achievable by varying just the diameter makes it potentially the best geometry for linking conventional optical length scales with the nanoscale. Nevertheless, recent experiments have shown only modest enhancements in spontaneous emission [16, 17] and a practical implementation of nanoscale focusing with metal cylinders has yet to conclusively match predictions [26].

5.4. HPPs

This type of structure is particularly appealing due to its compatibility with integrated photonics systems, such as silicon on insulator-based photonics architectures. HPPs are capable of strong enhancements of spontaneous emission as well as overall energy confinement, making them attractive also for nano-scale focusing. At the same time, HPPs have favorable propagation characteristics showing significantly improved propagation distance for the same degree of confinement when compared with the other waveguides in this study. The hybrid plasmon waveguide is amenable to standard lithography and thin film deposition techniques, making it an attractive architecture for nano-optics research both in terms of technological applications and pure science.

Acknowledgments

This work was supported by AFOSR MURI (FA9550-04-1-0434) and NSF Nanoscale Science and Engineering Centre (DMI-0327077).

Appendix A. Relationship between the Purcell factor and the effective mode area, A_1

The first measure of field confinement, A_1, is related to the Purcell factor, which quantifies a mode's ability to enhance the spontaneous emission rate of a near-by atom. In the case of a waveguide, we equate the stored electromagnetic energy per unit length with the vacuum fluctuation energy, $1/2\hbar\omega$, and the one-dimensional density of states, $\rho_{1D} = n_g/(2\pi c)$ along the waveguide's degree of freedom,

$$A\langle W_{atm}\rangle = \frac{1}{2}\hbar\omega\frac{n_g}{2\pi c}, \tag{A.1}$$

where $n_g = \mathrm{d}[\omega \mathrm{Re}\{\beta/k_0\}]\,\mathrm{d}\omega$ is the group index of the waveguide mode. Here, we have assumed that the mode's energy is distributed over an area A, which will be our measure of confinement, while the vacuum fluctuation energy density at the atom is $\langle W_{atm}\rangle$. The angular brackets are to indicate that the field corresponds to that of the vacuum fluctuations. Similarly, for an atom in an unbounded medium of refractive index n, we equate the time averaged electromagnetic energy density, $n^2\varepsilon_0|\mathbf{E}_0|^2$ (noting that the electric and magnetic energy densities are equal), with the vacuum energy and the density of states in vacuum,

$$n^2\varepsilon_0\langle|\mathbf{E}_0|\rangle^2 = \frac{1}{2}\hbar\omega\frac{\omega^2 n^3}{\pi^2 c^3}. \tag{A.2}$$

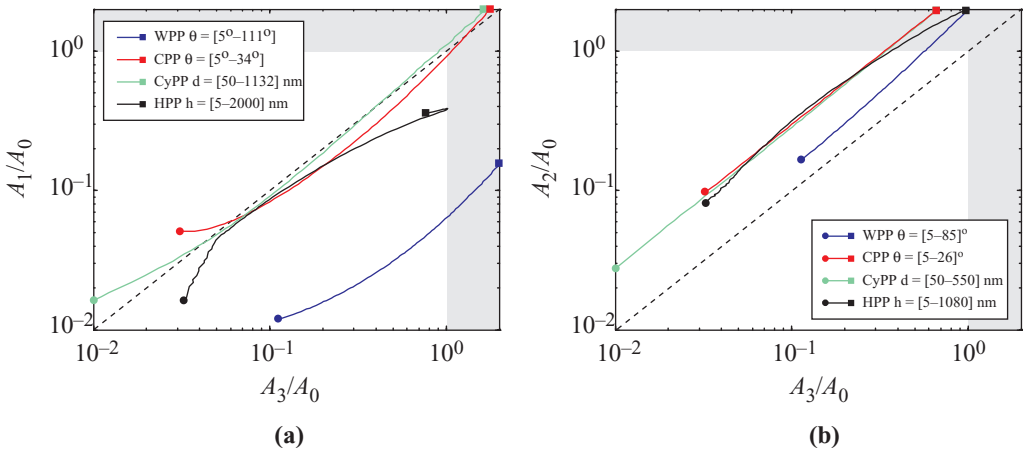

Figure B.1. Parametric plots of waveguide confinement: (a) $A_{1/2}$ versus A_1 and (b) $A_{1/2}$ versus A_2. The tip radius, $\rho = 10$ nm for both metal wedge and groove.

The Purcell factor is the ratio of the fluctuating electric field intensities of equations (A.1) and (A.2) [21]. When the emission medium in both vacuum and the waveguide share the same refractive index, n,

$$\langle W_{\text{atm}} \rangle = n^2 \varepsilon_0 \langle |\mathbf{E}_{\text{atm}}| \rangle^2 \frac{1}{2} \left[1 + \frac{\mu_0 \langle |\mathbf{H}_{\text{atm}}|^2 \rangle}{\varepsilon \langle |\mathbf{E}_{\text{atm}}|^2 \rangle} \right], \tag{A.3}$$

so that,

$$F_{\text{p}} = \frac{n_{\text{g}}}{n^2 \pi A} \left(\frac{\lambda}{2} \right)^2 2 \left[1 + \frac{\mu_0 \langle |\mathbf{H}_{\text{atm}}|^2 \rangle}{\varepsilon \langle |\mathbf{E}_{\text{atm}}|^2 \rangle} \right]^{-1}. \tag{A.4}$$

Taking $A_0 = (\lambda/2)^2$ to be the diffraction limited area of vacuum and placing the atom at the maximum of the field we find

$$F_{\text{p}} \simeq \frac{1}{\pi} \frac{n_{\text{g}}}{n^2} \frac{A_0}{A_1}. \tag{A.5}$$

Here, we have assumed that the electric and magnetic energy densities in the vicinity of the atom are approximately equal. This approximation is commonly made in the literature, however, it is only valid for cases of weak confinement. Despite this, the measure A_1 (equation (4)) is a good indication of a waveguide's ability to enhance spontaneous emission.

Appendix B. Comparison of the effective mode areas, A_1, A_2 and A_3

In this section, we expand on our analysis of the various effective mode areas that we defined in the main text.

Figures B.1(a) and (b) plot A_1 and A_2 against A_3, respectively. For CyPPs and CPPs, A_1 (figure B.1(a)) is approximately the same as A_3, and so represents about 50% of the mode's energy across a reasonably broad range of the respective waveguide confinement parameter. Consequently, for moderate confinement, A_1 provides a reasonable indication of both the Purcell effect and the total energy confinement in these waveguides. For strong confinement, A_1 and A_3 are very different for all the waveguide studied: for CyPPs and CPPs, A_1 represents more than

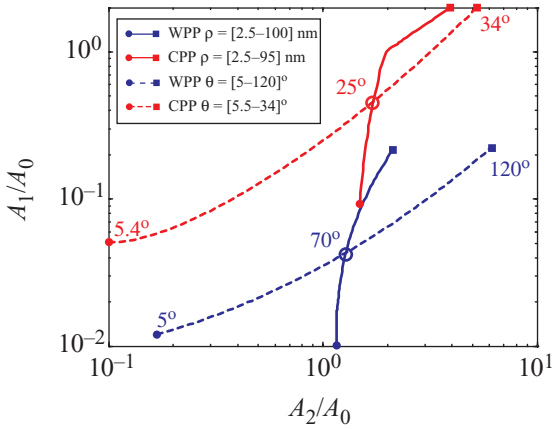

Figure B.2. Comparison of effective mode area, A_1 and A_2 in CPP and WPP waveguides parameterized by the tip radius, ρ (solid lines). Broken lines show the same comparison for $\rho = 10\,\text{nm}$ parameterized by the sidewall angle, θ.

half of a mode's energy, while for HPPs, it represents less. WPPs follow a completely different trend from the other waveguides. Based on these observations, A_1 is not a good measure of the electromagnetic energy confinement of an arbitrary plasmonic mode. Strictly, it should be used as a measure of the Purcell effect.

In contrast, the A_2 measure (figure B.1(b)) is more consistent for all the waveguides examined. In all cases, A_2 represents more than 50% of a mode's energy across the full range of parameterization and for all the plasmonic waveguides studied. The principal difference between A_2 and A_3 appears to be a constant factor; however, a closer examination shows that this is not strictly the case. While CPPs and CyPPs follow the trend $A_2 \approx 3A_3$, WPPs and HPPs have factors that vary between 1.5–2 and 2–3 respectively. Care is needed when using A_2 to compare different plasmonic waveguides: for example, A_2 represents less of the WPP's energy than the other modes, giving an effective area that is about two times smaller.

All four measures give very different effective mode areas for WPPs. A_1 and A_2 consistently represent a smaller proportion of a WPP's overall energy, which give them a distinctive confinement characteristics to the other waveguides. To examine this further, figure B.2 shows the comparison of A_1 and A_2 for CPPs and WPPs, but this time with a variable tip radius, $\rho = [2.5, 100]\,\text{nm}$. Sharper tips increase A_1 in both waveguides with a much smaller apparent change in A_2. Therefore, the tip radius effectively controls the local field enhancement, having only a weak effect on the overall confinement of electromagnetic energy. For example, the difference in A_3 between $\rho = 100\,\text{nm}$ and $\rho = 2.5\,\text{nm}$ for WPPs is only a factor of 2. On the other hand, the field near the tip is localized to such an extent that the A_1 measure is increased by more than 20 times for the same change of tip radius. CPPs follow a similar trend, although for very large tip radii ($\rho > 25\,\text{nm}$) confinement is lost more rapidly than for WPPs. This is likely to be due to the way in which confinement is lost in these geometries: when CPPs lose confinement they must de-localize into the groove, while WPPs can spread out radially in directions that are far less limited.

References

[1] Barnes W L, Dereux A and Ebbesen T W 2003 Surface plasmon sub-wavelength optics *Nature* **424** 824–30

[2] Pfieffer C A, Economou E N and Ngai K L 1974 Surface polaritons in a circularly cylindrical interface: surface plasmons *Phys. Rev.* B **10** 3038–51

[3] Takahara J, Yamagishi S, Taki H, Morimoto A and Kobayashi T 1997 Guiding of a one-dimensional optical beam with nanometer diameter *Opt. Lett.* **22** 475–7

[4] Jung J, Sondergaard T and Bozhevolnyi S I 2007 Theoretical analysis of square surface plasmon-polariton waveguides for long-range polarization-independent waveguiding *Phys. Rev.* B **76** 035434

[5] Maier S A, Kik P G, Atwater H A, Meltzer S, Harel E, Koel B E and Requicha A A G 2003 Local detection of electromagnetic energy transport below the diffraction limit in metal nanoparticle plasmon waveguides *Nat. Mater.* **2** 229–32

[6] Pile D F P, Ogawa T, Gramotnev D K, Okamoto T, Haraguchi M, Fukui M and Matsuo S 2005 Theoretical and experimental investigation of strongly localized plasmons on triangular metal wedges for subwavelength waveguiding *Appl. Phys. Lett.* **87** 061106

[7] Moreno E, Rodrigo S G, Bozhevolnyi S I, Martin-Moreno L and Garcia-Vidal F J 2008 Guiding and focusing of electromagnetic fields with wedge plasmon polaritons *Phys. Rev. Lett.* **100** 023901

[8] Boltasseva A, Volkov V S, Nielsen R B, Moreno E, Rodrigo S G and Bozhevolnyi S I 2008 Triangular metal wedges for subwavelength plasmon-polariton guiding at telecom wavelengths *Opt. Express* **16** 5252–60

[9] Pile D F P and Gramotnev D K 2004 Channel plasmon-polariton in a triangular groove on a metal surface *Opt. Lett.* **29** 1069–71

[10] Bozhevolnyi S I, Volkov V S, Devaux E and Ebbesen T W 2005 Channel plasmon-polariton guiding by sub-wavelength metal grooves *Phys. Rev. Lett.* **95** 046802

[11] Bozhevolnyi S I, Volkov V S, Devaux E, Laluet J-Y and Ebbesen T W 2006 Channel plasmon subwavelength waveguide components including interferometers and ring resonators *Nature* **440** 508–11

[12] Oulton R F, Sorger V J, Genov D A, Pile D F P and Zhang X 2008 A hybrid plasmonic waveguide for subwavelength confinement and long-range propagation *Nat. Photonics* **2** 496–500

[13] Huang M H, Mao S, Feick H, Yan H, Wu Y, Kind H, Weber E, Russo R and Yang P 2001 Room-temperature ultraviolet nanowire nanolasers *Science* **292** 1897–9

[14] Hill M T *et al* 2007 Lasing in metallic-coated nanocavities *Nat. Photonics* **1** 589–94

[15] Conway J A, Sahni S and Szkopek T 2007 Plasmonic interconnects versus conventional interconnects: a comparison of latency, crosstalk and energy costs *Opt. Express* **15** 4474–84

[16] Fedutik Y, Temnov V V, Schöps O, Artemyev M V and Woggon U 2007 Exciton-plasmon-photon conversion in plasmonic nanostructures *Phys. Rev. Lett.* **99** 136802

[17] Akimov A V, Mukherjee A, Yu C L, Chang D E, Zibrov A S, Hemmer P R, Park H and Lukin M D 2007 Generation of single optical plasmons in metallic nanowires coupled to quantum dots *Nature* **450** 402–6

[18] Johnson P B and Christy R W 1972 *Phys. Rev.* B **6** 4370

[19] Snyder A W and Love J D 1983 *Optical Waveguide Theory* (London: Chapman and Hall)

[20] Purcell E M 1946 Spontaneous emission probabilities at radio frequencies *Phys. Rev.* **69** 681

[21] van Exter M P, Nienhuis G and Woerdman J P 1996 Two simple expressions for the spontaneous emission factor β *Phys Rev.* A **54** 3553–8

[22] Agrawal G P 2001 *Nonlinear Fibre Optics: Principles and Practice* 3rd edn (New York: Academic)

[23] Buckley R and Berini P 2007 Figures of merit for 2D surface plasmon waveguides and application to metal stripes *Opt. Express* **15** 12174–82

[24] Babadjanyan A J, Margaryan N L and Nerkararyan Kh V 2000 Superfocusing of surface polaritons in the conical structure *J. Appl. Phys.* **87** 3785–8

[25] Stockman M I 2004 Nanofocusing of optical energy in tapered plasmonic waveguides *Phys. Rev. Lett.* **93** 137404

[26] Ropers C, Neacsu C C, Elsaesser T, Albrecht M, Raschke M B and Lienau C 2007 Grating-coupling of surface plasmons onto metallic tips: a nanoconfined light source *Nano Lett.* **7** 2784–8